Original research

Pathological alternations of mediastinal fat-associated lymphoid cluster and lung in a streptozotocin-induced diabetic mouse model

Yaser Hosny Ali Elewa[1,2,*], Osamu Ichii[2,3], Teppei Nakamura[2,4], Yasuhiro Kon[2]

[1)] Department of Histology and Cytology, Faculty of Veterinary Medicine, Zagazig University, Zagazig, Egypt

[2)] Laboratory of Anatomy, Department of Basic Veterinary Sciences, Faculty of Veterinary Medicine, Hokkaido University, Sapporo, Japan

[3)] Laboratory of Agrobiomedical Science, Faculty of Agriculture, Hokkaido University, Sapporo, Japan

[4)] Department of Biological Safety Research, Chitose Laboratory, Japan Food Research Laboratories, Chitose, Japan

Correspondence:

Dr. Yaser Elewa, Laboratory of Anatomy, Basic Veterinary Sciences, Faculty of Veterinary Medicine, Hokkaido University, Kita18-Nishi 9, Kita-Ku, Sapporo, Hokkaido, 060–0818, Japan.

Tel.: +81–11–706–5188; Fax: +81–11–706–5189;

E-mail: y-elewa@vetmed.hokudai.ac.jp, yaserelewa@zu.edu.eg

Running title: Correlation between diabetes and the development of lung injury and MFALCs.

Abstract

Diabetes is a devastating global health problem and is considered a predisposing factor for lung injury progression. Furthermore, previous reports of the authors revealed the role of mediastinal fat-associated lymphoid clusters (MFALCs) in advancing respiratory diseases. However, no reports concerning the role of MFALCs on the development of lung injury in diabetes have been published. Therefore, the study aimed to examine the correlations between diabetes and the development of MFALCs and the progression of lung injury in a streptozotocin-induced diabetic mouse model. Furthermore, immunohistochemical analysis for immune cells ($CD3^+$ T-lymphocytes, $B220^+$ B-lymphocytes, $Iba1^+$ macrophages, and $Gr1^+$ granulocytes), vessels markers ($CD31^+$ endothelial cells and LYVE-1^+ lymphatic vessels “LVs”), and inflammatory markers (TNF-α and IL-5) was performed. In comparison to the control group, the diabetic group showed lung injury development with a significant increase in MFALC size, immune cells, LVs, and inflammatory marker, and a considerable decrease of $CD31^+$ endothelial cells in both lung and MFALCs was observed. Furthermore, the blood glucose level showed significant positive correlations with MFALCs size, lung injury, immune cells, inflammatory markers, and LYVE-1^+ LVs in lungs and MFALCs. Thus, we suggested that the development of MFALCs and LVs could contribute to lung injury progression in diabetic conditions.

Keywords: Diabetes, lung injury, streptozotocin, mediastinal fat-associated lymphoid cluster, lymphatic vessels, immune cells

Introduction

Fat-associated lymphoid clusters (FALCs) are non-encapsulated lymphoid clusters found to be in direct contact with the surrounding adipocytes. FALCs have been reported mainly in association with the mesenteric and mediastinal fat tissues in healthy humans and mice. They are named mesenteric FALCs (Moro, et al., 2010) and mediastinal FALCs “MFALCs” (Elewa, et al., 2014), respectively. Furthermore, the development of such clusters has been demonstrated to be associated with inflammation (Benezech, et al., 2015; Elewa, et al., 2018). Yet, the literature does not report any study concerning the effect of metabolic diseases on the development of MFALCs.

Diabetes mellitus (DM) is a metabolic disease characterized by persistent hyperglycemia, with evidence of the development of acute lung injury/acute respiratory distress syndrome (Honiden & Gong, 2009; Zheng, et al., 2017).

It has previously been revealed that the histopathological features of lung injury in several mice models include accumulations of mononuclear cells, thickening of the interalveolar septa, collapsed alveoli, and increased collagen fiber deposition in the interalveolar septa, which may even lead to severe lung fibrosis replacing the normal lung architectures (Elewa, et al., 2016; Elewa, et al., 2018). Furthermore, a significantly positive correlation was observed between MFALCs development and lung injury pathogenesis in several mouse models. These included genetic autoimmune diseases (Elewa, et al., 2016; Elewa, et al., 2017); septic condition such as bleomycin induced-pneumonitis (Elewa, et al., 2018); and aseptic infections such as Mycoplasma pulmonis (Boonyarattanasoonthorn, et al., 2019). However, the pathological alternations of MFALCs and their possible role in lung injury pathogenesis in DM are not clarified.

FALCs mainly comprised macrophages, lymphocytes with no distinguished B and T cell zonation, and few granulocytes (Elewa, et al., 2014; Moro, et al., 2010). Also, several Th2 cytokines (such as interleukin 4 “IL-4”, IL-5, and IL13) have been reported to be expressed by FALC c-Kit^{+}Sca-1^{+} cells (Moro, et al., 2010). Additionally, an *in-vitro* study revealed that the IL-5 regulates B-cell antibody production (Sonoda, et al., 1989). Besides, the role of tumor necrosis

factor (TNF) receptors (TNFR1 and TNFR2) in FALC formation has been explicated. In contrast, a defective appearance of FALCs has been revealed in mice lacking such receptors (*Tnfrsf1a*$^{-/-}$*Tnfrsf1b*$^{-/-}$ mice) (Benezech, et al., 2015). Also, it has been shown that the proinflammatory cytokines, including TNF-α and IL in the lung, act as critical modulators of inflammation in the pathogenesis of lung injury development (Malaviya, et al., 2017).

Interestingly, FALCs have been reported to be highly vascularized structures and are found in close association with blood vessels (Benezech, et al., 2015; Moro, et al., 2010). Additionally, the role of lymphatic vessels and high endothelial venules (HEVs) in the development of such clusters in different strains of mice has been previously reported (Elewa, et al., 2014). Such HEVs have been reported as specialized types of post-capillary venules required for lymphocyte trafficking (Buscher, et al., 2016; Rangel-Moreno, et al., 2009). Additionally, there is increasing evidence suggesting that the lung microangiopathy development in diabetic patients is considered a predisposing factor for the development of lung injury (Pitocco, et al., 2012; Sandler, 1990).

In this report, the authors examined the morphology of MFALCs after diabetic induction by streptozotocin (STZ) in C57BL/6N (B6) mice. It was hypothesized that the alterations in MFLAC development could play a significant role in the pathogenesis of lung injury progression following diabetic induction. The authors also suggest that LVs could be considered potential avenues for recruiting immune cells into the lungs and into and out of MFALCs. This thus leads to the progression of lung injury and MFALCs development. The authors also postulated that the damaged endothelial cells could contribute to lung injury progression with less effect on MFALCs development.

Material and Methods

Experimental animals and ethics statement

Healthy, male B6 mice (aged eight weeks) were purchased from Japan SLC, Inc. (Shizuoka, Japan) and maintained under specific pathogen-free conditions to be used as per the experimental design. The investigators adhered to the Guide for the Laboratory Animal Care and Use approved by the Institutional Animal Care and Use Committee of the Graduate School of Veterinary Medicine, Hokkaido University (approval No. 15–0079).

Experimental design

B6 mice were administered intraperitoneal (i.p.) injection of STZ (Calbiochem, San Diego, CA, USA) dissolved in 0.05 M sodium citrate buffer (CB) (pH 4.5) at a dose of 40 mg/kg body weight (BW), which represented the diabetic group. The remaining mice were injected CB and comprised the control group (n = 5 mice/group). The protocol of STZ- diabetic induction was performed according to the previous report (Ichii, et al., 2010; Tamura, et al., 2005). Briefly, mice of either the diabetic or control groups received two rounds of i.p. injections, i.e., either STZ or CB (for five consecutive days/round), respectively. The first round was completed at eight weeks, and the second round was injected at 12 weeks of age. The sampling was done at 15 weeks of age (Figure 1a).

Blood glucose level analysis and sampling for histopathological observation

At 15 weeks of age, mice from both control and the diabetic group were weighed and sacrificed under deep anesthesia (using a mixture of midazolam at a dose of 4.0 mg/kg, medetomidine at a dose of 0.3 mg/kg, and butorphanol at a dose of 5.0 mg/kg). Blood glucose level was measured using Medisafe Fit blood glucose meters and its TIPs (MEDISAFE Fit Smile, TERUMO, Tokyo, Japan) according to the manufacturer's instructions. Mice were considered diabetic when the blood glucose level was ≥ 200 mg/dL. On the other hand, the control group's blood glucose level was

found to be ≤ 100 mg/dL (Figure 1b). The pancreas, mediastinal fat tissue, and lung were immediately fixed in 4% paraformaldehyde overnight at 4º C for histopathological analysis. Also, the spleen of mice in each group was weighted, and the average spleen/BW in each group was calculated.

Tissue preparation for histopathological observation

Following overnight fixation, the specimens were washed with distilled water and subjected to dehydration in ascending graded ethanol. The samples were then cleared in xylene (3 changes/30 min each) and embedded in melted paraffin (3 changes/60 min each). Paraffin blocks were prepared, cut using microtome at three µm thickness, and subjected to either routine histological staining or immunohistochemical staining following deparaffinization and hydration.

The sections were stained with either hematoxylin and eosin (H&E) or Masson's trichrome (MT) to detect the degree of lung fibrosis for routine histological examination. To detect different types of collagen in lung, both groups' lung sections were immunostained with rabbit polyclonal anti-collagen I antibody (ab21286, abcam, Tokyo, Japan) diluted at 1:300, and rabbit polyclonal anti-COL3A1 (22734-1-AP, Proteintech, Manchester, United Kingdom) diluted at 1:1000. For pancreatic sections, immunohistochemical staining was performed to detect insulin positive beta cells using rat monoclonal anti-insulin antibody (MAB1417, diluted at 1:300, R&D, Funakoshi Co., Ltd., Tokyo, Japan). Furthermore, to detect different immune cells (B- lymphocytes, T-lymphocytes, macrophages, and granulocytes) within the MFALCs and lung tissue, immunohistochemical staining was performed using rat monoclonal anti-B220 at 1:1600 dilution (Cat. No. CL8990NA, Cedarlane, ON, Canada), rabbit monoclonal anti-CD3 at 1:200 dilution (Cat. No. 413601, Nichirei, Tokyo, Japan,), rabbit anti-Iba1 at 1:1000 dilution (Cat. No. 019–19741, Fujifilm Wako, Osaka,

Japan), and rat monoclonal anti-Gr-1 antibodies at 1:800 dilution (Cat. No. MAB1037, R and D system, MN, USA), respectively. Furthermore, for the analysis of the degree of development of vasculature within MFALCs and lung tissue, immunohistochemical staining was performed using rat monoclonal anti-peripheral node addressin PNAd at 1:500 dilution (Cat. No.12, Biolegend, San Diego, CA, USA), rabbit anti-LYVE-1 at 1:500 dilution (Cat. No. AG-25T- 0103, AdipoGen, San Diego, CA, USA), and rabbit monoclonal anti-CD31 antibodies at 1:100 dilution (Cat. No. Ab28364, Abcam), to detect the expression of HEVs, LVs, and ECs lining the blood capillaries and vessels. Additionally, immunohistochemistry was performed to detect the expression pattern of the proinflammatory cytokines in both MFALCs and lung tissue using rabbit anti-TNF-α (Cat. No. ab6671, Abcam) and IL-5 (LS-C177535–100, Life Span Bioscience) antibodies (at dilution of 1:200, and1:500, respectively). The immunohistochemical staining was performed as per the author's previous report (Elewa, et al., 2016; Elewa, et al., 2014; Elewa, et al., 2018). Except for the immunohistochemical staining of Gr-1, CD3, and CD31, the antigen retrieval was performed by heating the section at 105 °C for 15 min in 10 mM CB (pH 6.0) solution. For Gr-1, the sections were incubated at 37 °C for 5 min in 0.1% pepsin/0.2 M HCl. For CD3 and CD31, antigen retrieval was performed by heating the section at 110 °C for 20 min in Tris solution.

Morphometrical measurements:

For histomorphometry, photomicrographs were captured from the H&E-, MT, and immune- stained sections (three different tissue sections from mice of each group) at 200x magnification using a BZ-X710 microscope. They were subjected to the following measurements using the BZ-X analyzer (Keyence, Osaka, Japan) software:

(a) The percentage of ratios for islets area/pancreatic area; lymphoid clusters (LCs) area/total mediastinal fat tissue (MFT) area; HEVs area/LCs area; LVs area/LCs area; LVs area/lung field area; $CD31^+$ capillary endothelial cells area/LCs area; and $CD31^+$ capillary endothelial cells area/lung field area. Briefly, using the BZ-X analyzer, the

areas of the pancreatic islet, LCs, HEVs, LVs, $CD31^+$ blood capillary were measured in the captured photographs and divided into the corresponding field area of either pancreas, MFT, LCs, or lung. The average ratios were then reported and compared among the groups, as previously reported (Elewa, et al., 2014).

(b) The percentage of aniline $blue^+$ collagen areas was measured from photographs of MT-stained sections using the BZ-X analyzer and divided to that of the corresponding field area of lung sections as previously revealed (Elewa, et al., 2018).

(c) The percentages of ratios for the positive area of immune cells (T-lymphocytes, B-lymphocytes, macrophages, and granulocytes), TNF- α, and IL-5^+ cells/LCs area was measured in three different MFT sections/mice. To calculate the positive area ratios for the immunopositive cells, the BZ-X analyzer was used to measure the positive area for different immunopositive cells and divided it into the field area. Then the averages of the percentages were calculated and compared between the two groups.

(d) The percentage of positive index ratios for $insulin^+$ β- cells/islet area, immune cells/lung field, TNF- α, IL-5^+ cells/lung field, and $CD31^+$ endothelial cells/large blood vessels within the lung sections were compared among both the groups. The number of immunopositive cells in five random fields within each of the three different sections (at 200× magnification) was counted to calculate the positive index ratio. Then, the number was divided by the area of the same corresponding field. Next, the average index ratios/group was calculated and compared among both the groups.

Furthermore, the degree of lung injury among both the control and diabetic groups was analyzed by comparing the average score of the grades for lung fibrosis based on a scale criterion (Ashcroft, et al., 1988). Briefly, grading of different microscope fields was detected on a scale from zero to 8 (grade 0: Normal lung structure; grade 1: Slight thickening of the alveolar wall with few cellular infiltrations; grade 3: Slight thickening of the alveolar wall with moderate cellular infiltrations; grade 5: Numerous cellular infiltrations with mild fibrosis, and clear damage to the

lung architecture; grade 7: Severe damage of lung tissue with clear fibrous masses; grade 8: Total replacement of lung tissue with fibrous tissue). The average of odd number scores for different microscopic fields/lung sections was recorded. The intervening even-numbered score was considered in case of any suspicion while deciding between two odd-numbered grades.

2.6. Statistical analysis:

To compare the differences between diabetic and control groups, the Mann–Whitney *U*-test was performed, and statistical significance was determined at p values ≤ 0.05. All numerical data have been presented as mean ±standard error (SE). Moreover, to assess the correlation between two variables, Spearman's correlation was used (*significant value, $p \leq 0.05$; and ** highly significant value, $p \leq 0.01$).

Results

Diabetic index

Both blood glucose level and histoplanimetrical measurements of the ratio of islet area/pancreatic tissue, as well as insulin+ β cell index ratio (number of insulin+β cell/islet area), were analyzed as diabetic indices to confirm the diabetic induction following two rounds of STZ IP injection (5 consecutive days/round). The blood glucose level was measured in the serum collected at 15 weeks of age in diabetic and control groups (Figure 1a). The diabetic group showed a significantly higher blood glucose level than the control group (Figure 1b). Moreover, immunohistochemical staining of insulin revealed fewer insulin-positive β cells in the diabetic group's pancreatic islets than that of the control group (Figure 1c). Histoplanimetrical measurements of the pancreatic islet in the diabetic group revealed a significant decrease in its size (ratio of islet area/pancreatic area) (Figure 1d) and the insulin^{+} β cell index ratio as compared to the control group.

Effect of diabetic induction on the morphological features of MFALCs and spleen/BW ratio

In order to investigate the effect of diabetes induction on the body immune status, the LC/MFT area ratio (as localized intrathoracic effect) and the spleen/BW ratios (as generalized effect) were analyzed. Examination of H&E-stained mediastinal fat tissue sections revealed an increase in the sizes of MFALCs in the diabetic group compared to those in the control group (Figure 2a). The LC/MFT area ratio among both groups was also compared to investigate the degree of MFALCs development. Interestingly, the diabetic group revealed a significantly higher LC/MFT area ratio than the control groups (Figure 2b). On the other hand, no significant differences could be observed in spleen/BW ratios between the two groups (Figure 2c).

Effect of diabetic induction on the histopathological features of the lung

The lung tissue among diabetic and control groups was compared to examine the effect of

diabetes induction on lung lesions' progression. Analysis of H&E-stained lung sections in the control group revealed normal lung architecture with a thin alveolar wall, inter-alveolar septa, and a limited number of immune cell infiltrations. However, the diabetic group's lungs showed large accumulations of mononuclear cells, alveolar collapse, and some areas showed diffuse alveolar damage (Figure 3a). Furthermore, the MT staining of diabetic lung sections revealed numerous aniline blue^{+} collagen fibers accumulation specially around blood vessels, the bronchi, and interalveolar spaces with the presence of numerous congested blood vessels. However, only a few collagen fibers could be detected in the interalveolar spaces of the control group lung (Figure 3b). Histopathological quantification of the degree of lung injury was done using a standardized scoring system (Ashcroft, et al., 1988). Interestingly, the diabetic group showed a significantly higher lung injury score than the control group (Figure 3c). Furthermore, the percentage of aniline blue^{+} area of the diabetic group was significantly higher than that of the control group (Figure 3d). To detect different types of collagen deposition, the lung sections from both groups were immuno-stained with collagen I (Figure 4a) and col3A1 (Figure 4b) antibodies. Similar to the MT-stained lung sections, more positively stained collagen fibers deposition was mainly observed around the bronchi and large blood vessels of diabetic group than that of control group.

Effect of diabetic induction on the immune cell populations within MFALCs and infiltration into the lung

To determine the effect of diabetes on the immune cell populations within both MFALCs and lung tissue, immunohistochemical staining for B220-, CD3-, Iba1-, and Gr1- was performed. This staining was done to detect B-lymphocytes, T-lymphocytes, macrophages, and granulocytes, respectively. Immunohistochemical analysis B220-, CD3-, Iba1-, and Gr1-$^{+}$ cells within the MFALCs of the diabetic group revealed a significant increase (2.05, 1.46, 1.81, 5.37 fold, respectively) in the ratio of immune cell^{+} area/LCs area as compared to that of the control group (Figure 5a). Also, the diabetic group's lung showed more immune cell infiltration than that of the

control group. The percentages of immune cell$^+$ index ratio were compared among both groups to assess immune cell infiltrations into the lung. Interestingly, the diabetic group revealed a significantly higher positive immune cell density than the control group. The diabetic group also showed 4.03, 4.30, 3.30, 2.95-fold increase for the B220-, CD3-, Iba1-, and Gr1-$^+$ cell density, respectively, than that of the control group (Figure 5b).

Histopathological correlations between the diabetic index, and parameters of the lung and MFALCs

The correlations between diabetic index (blood glucose level, and Insulin$^+$ index ratio), and parameters of the lung (lung injury score, aniline blue$^+$ area, immune cells) and MFALCs (MFALCs size, immune cell populations of "B-lymphocytes, T-lymphocytes, macrophages, and granulocytes," and the ratio of HEVs area) was analyzed. As shown in Table 1, significantly positive correlations were observed between blood glucose and parameters of the lung and MFALCs (except for the HEVs within MFALCs, where a non-significantly positive correlation was observed). However, for the insulin$^+$ index ratio, significant negative correlations to MFALCs size, degree of lung injury, immune cells within MFALCs, and lung was indicated. Additionally, significant positive correlations were observed between the HEVs and MFALCs size, and immune cell populations within the MFALCs, as well as with lung parameters. Furthermore, a positive correlation was detected between lung aniline blue$^+$ area and immune cell populations with MFALCs. Such correlations showed significant differences with all immune cell populations except for the CD3$^+$ T-lymphocytes.

Immunohistochemical staining of the PNAd$^+$ HEVs, LYVE-1$^+$ LVs, and CD31$^+$ endothelial cells within MFALCs and lung

Immunohistochemical staining for PNAd was performed to determine the effect of

diabetic induction on HEVs in the MFALCs and the lungs. $PNAd^+$ HEVs were more abundant in the MFALCs of the diabetic group than that of the control group (Figure 6a). However, such $PNAd^+$ HEVs were not detected in the lung of either group (data not shown). Quantitative measurements of the $PNAd^+$ HEVs area ratio within the MFALCs of the diabetic group showed significantly higher percentages than that of the control group (Figure 6b).

Immunohistochemistry of the LYVE-1^+ LVs demonstrated more developed LVs in both MFALCs and the diabetic group's lung than that of the control group (Figure 7a). Similarly, the morphometrical measurements of the ratio of LYVE-1^+ LVs area within both MFALCs (Figure 7b) and lung (Figure 7c) indicated significantly higher percentages in the diabetic group than that in the control group.

To compare the abundance of blood capillaries in the MFALCs and the lungs of both diabetic and control groups, immunohistochemical analysis for $CD31^+$ endothelial cells was performed. Interestingly, the MFALCs and lung of the diabetic group showed less $CD31^+$ blood capillary than that of the control group. Also, few $CD31^+$ endothelial cells were observed in the large blood vessels of the diabetic group lung than the control group (Figure 8a). Interestingly, the quantitative index of the percentages of $CD31^+$ capillary area ratio in the MFALCs (Figure 8b) and the lungs (Figure 8c) of the diabetic group was significantly decreased compared to that in the control group. Furthermore, a significant decrease in the index ratio of $CD31^+$ in endothelial cells/blood vessel walls within the diabetic lung was observed compared to that in the control group (Figure 8d).

Immunohistochemical staining of the proinflammatory cytokine (TNF-α, and IL-5) positive cells within MFALCs and lung

Immunohistochemical staining for the TNF-α^+ cells in MFALCs revealed that most of the immune cells within the MFALCs reacted positively to TNF-α and the MFALCs of the diabetic group showed more abundantly positive cells (Figure 9a). Histomorphometrically, a significantly higher

TNF-α$^+$ area ratio was observed in the MFALCs of the diabetic group as compared to that of the control group (Figure 9b). Similarly, the control group's lung showed few TNF-α+ cells, but more abundant TNF-α+ cells (mainly macrophages, neutrophils, and lymphocytes) were observed in the diabetic group's lung. Furthermore, a positive TNF-α reaction was observed in the endothelial cells lining the blood vessels and epithelial lining of the bronchiole in the diabetic group (Figure 9a). TNF-α$^+$ index ratio in the diabetic group's lungs was significantly higher than those in the control group (Figure 9c).

Immunohistochemical staining for the IL-5$^+$cells in the MFALCs revealed that most of the immune cells within the MFALCs reacted positively to IL-5 and the MFALCs of the diabetic group showed higher IL-5$^+$ cells than the control group (Figure 10a). Quantitative measurement of the IL-5$^+$ area ratio in the MFALCs of the diabetic group revealed a higher percentage than the control group, though the difference was non-significant (Figure 10b). Also, more abundant IL-5$^+$ cells were observed in the diabetic lung than that of the control group. The immunopositivity was mainly observed in macrophage, neutrophils, and lymphocytes (Figure 10a). Interestingly, a significantly higher IL-5+ index ratio was observed in the diabetic group's lungs than those in the control group (Figure 10c).

Histopathological correlations between blood glucose level and both vessel areas and proinflammatory markers in the MFALCs and lung of diabetic and control groups

The pathological correlations between blood glucose level and vessel areas (CD31$^+$ blood capillaries and LYVE-1$^+$ LVs) in MFALCs and lung were examined (Figure 11a). Significantly negative correlations were observed between blood glucose level and blood capillary areas within both MFALCs and lungs. However, significant positive correlations were reported between blood glucose levels and blood capillaries in both MFALCs and lungs.

Furthermore, the blood glucose level showed a significantly positive correlation with proinflammatory cytokines (TNF-α and IL-5) within both MFALCs and lung (Figure 11b).

Discussion

DM is a chronic metabolic disease characterized by an abnormality in carbohydrate metabolism and an increased blood glucose level. This may be due to impaired body ability to produce or respond to the insulin hormone and is classified into either type 1 or type 2 DM, respectively (Bajpai, 2018; Kolluru, et al., 2012). STZ is an alkylating agent, previously used as a chemotherapeutic substance for treating pancreatic islet tumors because of its preferential accumulation in pancreatic β-cells via the GLUT2 transporter system, which led to the cytotoxicity of β-cells (Eleazu, et al., 2013; Ventura-Sobrevilla, et al., 2011). STZ is one of the most widely used diabetogenic drugs that induce diabetes in experimental animal models because of their selectively damaging effect on β-cells (Akbarzadeh, et al., 2007; Goud, et al., 2015).

In addition to the toxic effect of STZ on β-cells, STZ toxicity has also been reported from other vital organs (including kidney, eye, nerves, and brain), leading to the development of diabetic nephropathy, retinopathy, neuropathy, and cerebrovascular diseases (Fong, et al., 2004; Kario, et al., 2005; Tervaert, et al., 2010; Tesfaye, et al., 2005). On the other hand, and unlike other vital organs, the lungs have been reported to be less sensitive to the toxicity of STZ (Samarghandian, et al., 2014). Despite that fact, pulmonary dysfunction and dyspnea have been associated with Type I DM (Scano, et al., 1999). Interestingly, it has been established that the progression of lung damage and asthma associated with DM is owed to an increased level of inflammatory mediators and oxidative stress in the bronchoalveolar lavage fluid (Samarghandian, et al., 2014).

The current investigation indicated the development of lung injury and fibrosis in the diabetic group compared to the control group. Similarly, recent reports revealed that alteration in the genes involved in stress and collagen leads to the lungs' functional impairment in streptozotocin-induced diabetic rats (Talakatta, et al., 2018; van Lunteren, et al., 2014). Also, pulmonary interstitial fibrosis has been reported to develop in STZ-induced diabetic rat following hyperglycemia (Talakatta, et al., 2018; Zou, et al., 2017). Furthermore, the author's previous reports have suggested the possible role of MFALCs in the pathogenesis of lung injury and fibrosis in both

autoimmune disease mice model (Elewa, et al., 2016) and bleomycin-induced pneumonitis mice model (Elewa, et al., 2018). However, the role of MFALCs in the progression of lung injury in the STZ-induced diabetic mice model and the effect of diabetes on the pathological alterations of MFALCs is not yet clarified. Interestingly, more developed MFALCs were observed in the diabetic group than that of the control group in the present study population. Besides, a significantly positive correlation was observed between the progression of lung injury and the size of MFALCs and the blood glucose level as a diabetic index, suggesting that MFALCs could play a role in the pathogenesis of lung lesions in DM. However, further investigations are required to clarify if reprogramming MFALCs through targeting some immune cells/ LVs or HEVs could help in controlling the lung injury development.

The present study revealed a significant increase in the quantitative index of immune cells (mainly for B-lymphocytes, T-lymphocytes, and macrophages) and the TNF-α and IL-5^{+}cells in both MFALCs and lung of the diabetic group as compared to the control group. Similarly, intense cellular infiltration has been reported in the interstitial tissue of the lungs of diabetic group rats compared to the control rats (Talakatta, et al., 2018). Primarily, macrophages and monocytes produce TNF- α (Aggarwal, et al., 2012; Suzuki, et al., 2013). Interestingly, the role of adipose tissue macrophages in FALCs formation has been reported. Such a function is because the adipose tissue macrophages are considered the primary TNF source, which stimulates TNF receptor on the stromal cells (Benezech, et al., 2015). Furthermore, other functions of TNF-α have been illustrated, including promoting leukocyte accumulation and tissue remodeling (Aggarwal, 2003; Mukhopadhyay, et al., 2006). Additionally, IL-5 has been reported to regulate B1 cells' self-renewal and B cell antibody production (Erickson, et al., 2001).

Angiopathy or abnormal angiogenesis is one of DM's major complications (Martin, et al., 2003; Xu, et al., 2012). Interestingly, a complicated alveolar-capillary network was observed in the healthy lung. Microvascular damage was observed in such capillary network in the lung in association with DM and led to an increased risk of several pulmonary diseases (De Santi, et al.,

2017; Ehrlich, et al., 2010). The present study revealed a capillary defect in the MFALCs and lung of the diabetic group. Simultaneously, a significant decrease in the CD31+ capillary endothelial lining cells of the diabetic group than the control group was also found. Similarly, endothelial cell dysfunction has been reported in patients with DM (Kolluru, et al., 2012).

On the other hand, the MFALCs and lung of the diabetic group showed a significant increase in the LVs area ratios than that of the control group in the present study. Also, a significantly positive correlation between blood glucose level and the quantitative index of LVs was observed. Interestingly, it has been clarified that the pulmonary LVs could transport a larger number of immune cells than do other LVs in different organs because of the lack of smooth muscle cell coverage of pulmonary collecting LVs, and thus showed more permeability with facilitated cellular extravasation (Reed, et al., 2019). Therefore, the authors suggest that the LV development observed in the MFALCs and lungs of the diabetic group could play a significant role in immune cell trafficking among them, and in turn, provide a possible mechanism in lung injury progression associated with DM induction.

HEVs are specialized post-capillary venules that play an essential role in lymphocyte migration into and out of the lymph nodes, tonsils, Peyer's patches, and mucosa-associated lymphoid tissue (MALT) as secondary lymphoid structures (Girard & Springer, 1995). Additionally, previous studies by the authors have revealed the role of HEVs in MFALC development in both healthy (Elewa, et al., 2014) and diseased (Elewa, et al., 2016; Elewa, et al., 2018) conditions. Similarly, the present study revealed more developed HEVs in the MFALCs of the diabetic group than in the control group. It showed a significantly positive correlation with MFALC development and lung injury progression, suggesting the possible role of such venules in the intrathoracic immune hemostasis associated with diabetic conditions.

Conclusion

We have investigated the effects of diabetes induction on the pathological alterations of MFALCs

and their possible role in lung injury progression. The diabetic group showed a significant increase in MFALCs size, immune cells, inflammatory cytokines, HEVs, and LVs area compared with the control group. Furthermore, significant positive correlations were observed between MFALCs size, and quantitative indices of MFALCs parameters, and both the degree of lung injury and parameters of the lung. The data also revealed significantly positive correlations between blood glucose levels and quantitative parameters of LVs and HEVs. A significantly negative correlation was observed between blood glucose level and quantitative parameters of blood capillaries. Therefore, the present study hypothesized the possible role of MFALCs development as an additional mechanism in the pathogenesis of lung injury progression in diabetic mice. However, further investigations are required to clarify various signals involved in the development of MFALCs and the possible role of different cell populations within MFALCs in the mechanism of lung injury progression following diabetic conditions. Understanding such signals and the role of various immune cells within MFALCs could provide some therapeutic approaches for advancing lung lesions associated with metabolic disorders such as diabetes by targeting MFALCs.

ACKNOWLEDGMENTS

This research was sponsored by Hokkaido University Tenure Track Program and a grant-in-aid for the Japan Society for the Promotion of Science KAKENHI (No 20K07420).

References

Aggarwal BB. (2003). Signalling pathways of the TNF superfamily: a double-edged sword. *Nature reviews. Immunology* **3** (9), 745-756.

Aggarwal BB, Gupta SC & Kim JH. (2012). Historical perspectives on tumor necrosis factor and its superfamily: 25 years later, a golden journey. *Blood* **119** (3), 651-665.

Akbarzadeh A, Norouzian D, Mehrabi M, Jamshidi S, Farhangi A, Verdi AA, Mofidian S & Rad BLJIJoCB. (2007). Induction of diabetes by streptozotocin in rats. **22** (2), 60-64.

Ashcroft T, Simpson JM & Timbrell V. (1988). Simple method of estimating severity of pulmonary fibrosis on a numerical scale. **41** (4), 467-470.

Bajpai S. (2018). Chapter 8 - Biological importance of Aloe vera and its active constituents. In *Synthesis of Medicinal Agents from Plants*, Tewari, A. and Tiwari, S. (Eds.), pp. 177-203. Elsevier.

Benezech C, Luu NT, Walker JA, Kruglov AA, Loo Y, Nakamura K, Zhang Y, Nayar S, Jones LH, Flores-Langarica A, McIntosh A, Marshall J, Barone F, Besra G, Miles K, Allen JE, Gray M, Kollias G, Cunningham AF, Withers DR, Toellner KM, Jones ND, Veldhoen M, Nedospasov SA, McKenzie ANJ & Caamano JH. (2015).

Inflammation-induced formation of fat-associated lymphoid clusters. *Nat Immunol* **16** (8), 819-+.

Boonyarattanasoonthorn T, Elewa YHA, Tag-El-Din-Hassan HT, Morimatsu M & Agui T. (2019). Profiling of cellular immune responses to Mycoplasma pulmonis infection in C57BL/6 and DBA/2 mice. *Infection, Genetics and Evolution* **73**, 55-65.

Buscher K, Wang H, Zhang X, Striewski P, Wirth B, Saggu G, Lütke-Enking S, Mayadas TN, Ley K, Sorokin L & Song J. (2016). Protection from septic peritonitis by rapid neutrophil recruitment through omental high endothelial venules. *Nature communications* **7**, 10828.

De Santi F, Zoppini G, Locatelli F, Finocchio E, Cappa V, Dauriz M & Verlato G. (2017). Type 2 diabetes is associated with an increased prevalence of respiratory symptoms as compared to the general population. *BMC pulmonary medicine* **17** (1), 101.

Ehrlich SF, Quesenberry CP, Jr., Van Den Eeden SK, Shan J & Ferrara A. (2010). Patients diagnosed with diabetes are at increased risk for asthma, chronic obstructive pulmonary disease, pulmonary fibrosis, and pneumonia but not lung cancer. *Diabetes care* **33** (1), 55-60.

Eleazu CO, Eleazu KC, Chukwuma S & Essien UN. (2013). Review of the mechanism of cell

death resulting from streptozotocin challenge in experimental animals, its practical use and potential risk to humans. *Journal of Diabetes & Metabolic Disorders* **12** (1), 60.

Elewa YH, Ichii O & Kon Y. (2016). Comparative analysis of mediastinal fat-associated lymphoid cluster development and lung cellular infiltration in murine autoimmune disease models and the corresponding normal control strains. *Immunology* **147** (1), 30-40.

Elewa YHA, Ichii O & Kon Y. (2017). Sex-related differences in autoimmune-induced lung lesions in MRL/MpJ-faslpr mice are mediated by the development of mediastinal fat-associated lymphoid clusters. *Autoimmunity* **50** (5), 306-316.

Elewa YHA, Ichii O, Otsuka S, Hashimoto Y & Kon Y. (2014). Characterization of mouse mediastinal fat-associated lymphoid clusters. *Cell and Tissue Research* **357** (3), 731-741.

Elewa YHA, Ichii O, Takada K, Nakamura T, Masum MA & Kon Y. (2018). Histopathological Correlations between Mediastinal Fat-Associated Lymphoid Clusters and the Development of Lung Inflammation and Fibrosis following Bleomycin Administration in Mice. *Frontiers in immunology* **9**, 271.

Erickson LD, Foy TM & Waldschmidt TJ. (2001). Murine B1 B cells require IL-5 for optimal T cell-dependent activation. *J Immunol* **166** (3), 1531-1539.

Fong DS, Aiello L, Gardner TW, King GL, Blankenship G, Cavallerano JD, Ferris FL & Klein R. (2004). Retinopathy in Diabetes. **27** (suppl 1), s84-s87.

Girard JP & Springer TA. (1995). High endothelial venules (HEVs): specialized endothelium for lymphocyte migration. *Immunology today* **16** (9), 449-457.

Goud BJ, Dwarakanath V & Chikka BJIJPPR. (2015). Streptozotocin-a diabetogenic agent in animal models. **3** (1), 253-269.

Honiden S & Gong MN. (2009). Diabetes, insulin, and development of acute lung injury. *Critical care medicine* **37** (8), 2455-2464.

Ichii O, Otsuka S, Sasaki N, Yabuki A, Ohta H, Takiguchi M, Hashimoto Y, Endoh D & Kon Y. (2010). Local overexpression of interleukin-1 family, member 6 relates to the development of tubulointerstitial lesions. *Laboratory Investigation* **90** (3), 459-475.

Kario K, Ishikawa J, Hoshide S, Matsui Y, Morinari M, Eguchi K, Ishikawa S & Shimada KJH. (2005). Diabetic brain damage in hypertension: role of renin-angiotensin system. **45** (5), 887-893.

Kolluru GK, Bir SC & Kevil CG. (2012). Endothelial dysfunction and diabetes: effects on

519 angiogenesis, vascular remodeling, and wound healing. *International journal of vascular*
520 *medicine* **2012**, 918267.

521 **Malaviya R, Laskin JD & Laskin DL**. (2017). Anti-TNFα therapy in inflammatory lung diseases.
522 *Pharmacol Ther* **180**, 90-98.

523 **Martin A, Komada MR & Sane DC**. (2003). Abnormal angiogenesis in diabetes mellitus.
524 *Medicinal research reviews* **23** (2), 117-145.

525 **Moro K, Yamada T, Tanabe M, Takeuchi T, Ikawa T, Kawamoto H, Furusawa J, Ohtani M,**
526 **Fujii H & Koyasu S**. (2010). Innate production of T(H)2 cytokines by adipose
527 tissue-associated c-Kit(+)Sca-1(+) lymphoid cells. *Nature* **463** (7280), 540-544.

528 **Mukhopadhyay S, Hoidal JR & Mukherjee TK**. (2006). Role of TNFalpha in pulmonary
529 pathophysiology. *Respir Res* **7** (1), 125.

530 **Pitocco D, Fuso L, Conte EG, Zaccardi F, Condoluci C, Scavone G, Incalzi RA & Ghirlanda G**.
531 (2012). The diabetic lung--a new target organ? *Rev Diabet Stud* **9** (1), 23-35.

532 **Rangel-Moreno J, Moyron-Quiroz JE, Carragher DM, Kusser K, Hartson L, Moquin A &**
533 **Randall TD**. (2009). Omental milky spots develop in the absence of lymphoid

tissue-inducer cells and support B and T cell responses to peritoneal antigens. *Immunity* **30** (5), 731-743.

Reed HO, Wang L, Sonett J, Chen M, Yang J, Li L, Aradi P, Jakus Z, D'Armiento J, Hancock WW & Kahn ML. (2019). Lymphatic impairment leads to pulmonary tertiary lymphoid organ formation and alveolar damage. *J Clin Invest* **129** (6), 2514-2526.

Samarghandian S, Afshari R & Sadati AJTSWJ. (2014). Evaluation of lung and bronchoalveolar lavage fluid oxidative stress indices for assessing the preventing effects of safranal on respiratory distress in diabetic rats. **2014**.

Sandler M. (1990). Is the lung a 'target organ' in diabetes mellitus? *Archives of internal medicine* **150** (7), 1385-1388.

Scano G, Seghieri G, Mancini M, Filippelli M, Duranti R, Fabbri A, Innocenti F, Iandelli I & Misuri G. (1999). Dyspnoea, peripheral airway involvement and respiratory muscle effort in patients with type I diabetes mellitus under good metabolic control. *Clin Sci (Lond)* **96** (5), 499-506.

Sonoda E, Matsumoto R, Hitoshi Y, Ishii T, Sugimoto M, Araki S, Tominaga A, Yamaguchi N & Takatsu K. (1989). Transforming growth factor beta induces IgA production and acts

additively with interleukin 5 for IgA production. *J Exp Med* **170** (4), 1415-1420.

Suzuki J, Hamada E, Shodai T, Kamoshida G, Kudo S, Itoh S, Koike J, Nagata K, Irimura T & Tsuji T. (2013). Cytokine secretion from human monocytes potentiated by P-selectin-mediated cell adhesion. *International archives of allergy and immunology* **160** (2), 152-160.

Talakatta G, Sarikhani M, Muhamed J, Dhanya K, Somashekar BS, Mahesh PA, Sundaresan N & Ravindra PV. (2018). Diabetes induces fibrotic changes in the lung through the activation of TGF-β signaling pathways. *Scientific Reports* **8** (1), 11920.

Tamura J, Konno A, Hashimoto Y & Kon Y. (2005). Upregulation of renal renin-angiotensin system in mouse diabetic nephropathy. *The Japanese journal of veterinary research* **53** (1-2), 13-26.

Tervaert TWC, Mooyaart AL, Amann K, Cohen AH, Cook HT, Drachenberg CB, Ferrario F, Fogo AB, Haas M, de Heer E, Joh K, Noël LH, Radhakrishnan J, Seshan SV, Bajema IM & Bruijn JA. (2010). Pathologic Classification of Diabetic Nephropathy. **21** (4), 556-563.

Tesfaye S, Chaturvedi N, Eaton SE, Ward JD, Manes C, Ionescu-Tirgoviste C, Witte DR &

Fuller JHJNEJoM. (2005). Vascular risk factors and diabetic neuropathy. **352** (4), 341-350.

van Lunteren E, Moyer M & Spiegler SJBed. (2014). Alterations in lung gene expression in streptozotocin-induced diabetic rats. **14** (1), 5.

Ventura-Sobrevilla J, Boone-Villa VD, Aguilar CN, Román-Ramos R, Vega-Avila E, Campos-Sepúlveda E & Alarcón-Aguilar F. (2011). Effect of varying dose and administration of streptozotocin on blood sugar in male CD1 mice. *Proceedings of the Western Pharmacology Society* **54**, 5-9.

Xu L, Kanasaki K, Kitada M & Koya D. (2012). Diabetic angiopathy and angiogenic defects. *Fibrogenesis Tissue Repair* **5** (1), 13-13.

Zheng H, Wu J, Jin Z & Yan L-J. (2017). Potential Biochemical Mechanisms of Lung Injury in Diabetes. *Aging Dis* **8** (1), 7-16.

Zou X-Z, Gong Z-C, Liu T, He F, Zhu T-T, Li D, Zhang W-F, Jiang J-L, Hu C-PJPP & Therapeutics. (2017). Involvement of epithelial-mesenchymal transition afforded by activation of LOX-1/TGF-β1/KLF6 signaling pathway in diabetic pulmonary fibrosis. **44**, 70-77.

Figure 1. Experimental design and diabetic index: **(a)** Scheme of the experimental protocol showing schedule for intraperitoneal injection of either streptozotocin (STZ) or 0.05 M sodium citrate buffer (CB) in the diabetic group (DG) and control group (CG), respectively. **(b)** Blood glucose level. **(c)** Immunohistochemical staining of insulin^{+} β-cells. **(d)** Ratio of islet area/pancreatic area. **(e)** Index ratio of insulin-positive β-cells. Comparison between the control and diabetic groups (n = 5 mice in each group), analyzed by the Mann–Whitney *U*-test ($p \leq 0.05$). Statistically significant difference indicated by an asterisk (*). Values = mean ±SE.

Figure 2. Degree of MFALC development and spleen/body weight (BW) ratio: **(a)** H&E-stained mediastinal fat tissue (MFT), MFALCs (arrows). **(b)** the ratio of LC area/total MFT. **(c)** Percentage of the spleen/BW ratio. Comparison between the control and diabetic groups (n = 5 mice of each group), analyzed by the Mann–Whitney *U*-test ($p \leq 0.05$). Statistically significant difference indicated by an asterisk (*). Values = mean ±SE.

Figure 3. Histopathological features of the lungs **(a)** H&E-stained lung tissue. **(b)** Masson's trichrome staining of lung sections showing aniline blue^{+} collagen fibers (arrows), congested blood vessels (BV). **(c)** Lung injury score. **(d)** Comparison of the percentage of aniline blue^{+} collagen areas in lung tissues of diabetic and control groups. Comparison between the control and diabetic groups (n = 5 mice of each group), analyzed by the Mann–Whitney *U*-test ($p \leq 0.05$). Statistically significant difference indicated by an asterisk (*). Values = mean ±SE.

Figure 4. Collagen fibers deposition in the lungs. **(a)** Immunohistochemical staining of lung sections with the collagen I antibody. **(b)** Immunohistochemical staining of lung sections with the Col3A1 antibody. Diabetic group showed more deposition of collagen in the lung tissue around the large blood vessels and in the peri-bronchial tissue.

608

609 **Figure 5.** Immune cell populations in mediastinal fat-associated lymphoid clusters (MFALCs) and
610 lungs of diabetic and control groups. **(a)** Percentages of the immune cells (B-lymphocytes,
611 T-lymphocytes, macrophages, and granulocytes) positive area ratio in MFALCs. **(b)** Percentages of
612 the immune cells (B-lymphocytes, T-lymphocytes, macrophages, and granulocytes) positive index
613 ratio in lung tissues. Comparison between the control and diabetic groups (n = 5 mice of each
614 group), analyzed by the Mann–Whitney *U*-test ($p \leq 0.05$). Statistically significant difference
615 indicated by an asterisk (*). Values = mean ±SE.

616

617 **Figure 6.** The occurrence of high endothelial venules (HEVs) in MFALCs of diabetic and control
618 groups. **(a)** Immunohistochemical images depict $PNAd^+$ HEVs in MFALCs. Arrows indicate
619 $PNAd^+$ HEVs in MFALCs. **(b)** Percentage of the ratio of HEVs area within the MFALCs.
620 Comparison between the control and diabetic groups (n = 5 mice of each group), analyzed by the
621 Mann–Whitney *U*-test ($p \leq 0.05$). Statistically significant difference indicated by an asterisk (*).
622 Values = mean ±SE.

623

624 **Figure 7.** Lymphatic vessels (LVs) in MFALCs and lung of diabetic and control
625 groups. (**a)** Immunohistochemical staining for the LVs marker "LYVE-1. Arrows indicate LYVE-1^+
626 LVs. **(b)** Percentage of the LYVE-1+ LVs area ratio within the MFALCs. **(c)** Percentage of the ratio
627 of LYVE-1^+ LVs area within the lung. Comparison between the control and diabetic groups (n = 5
628 mice of each group), analyzed by the Mann–Whitney *U*-test ($p \leq 0.05$). Statistically significant
629 difference indicated by an asterisk (*). Values = mean ±SE.

630

631 **Figure 8.** Blood capillaries in MFALCs and lung of diabetic and control
632 group. (**a)** Immunohistochemical staining for the endothelial cell marker "CD31". Notice $CD31^+$
633 endothelial cells lining the blood capillaries (arrows) and blood vessels (black arrowheads), and

CD31 negative endothelial cells (red arrowheads). **(b)** Percentage of the ratio of LYVE-1$^+$ LVs area within the MFALCs. **(c)** Percentage of the ratio of CD31$^+$ capillary area within the lung. **(d)** Index ratio of CD31$^+$ endothelial cells/blood vessel wall within the lung. Comparison between the control and diabetic groups (n = 5 mice of each group), analyzed by the Mann–Whitney *U*-test ($p \leq 0.05$). Statistically significant difference indicated by an asterisk (*). Values = mean ±SE.

Figure 9. Analysis of the proinflammatory cytokines (TNF-α) in MFALCs and lung of diabetic and control groups. (**a)** Immunohistochemical staining for the TNF-α$^+$ cells in MFALCs and lungs. Notice the positive reaction for the neutrophils (black arrowheads), macrophages (red arrowheads), lymphocytes (green arrowheads), lining epithelium of bronchiolar wall (B). The diabetic lung showed TNF-α$^+$ reaction in the lining epithelium of bronchioles (black arrows) and the endothelial cells lining the blood vessels (red arrows). **(b)** Percentages of the TNF-α positive area ratio in MFALCs. **(c)** Percentages of the TNF-α positive index ratio in lung tissues. Comparison between the control and diabetic groups (n = 5 mice of each group), analyzed by the Mann–Whitney *U*-test ($p \leq 0.05$). Statistically significant difference indicated by an asterisk (*). Values = mean ±SE.

Figure 10. Analysis of the proinflammatory cytokines (IL-5) in MFALC and lung of diabetic and control group. (**a)** Immunohistochemical staining for the IL-5$^+$ cells in MFALCs and lungs. Notice the positive reaction for neutrophils (black arrowheads), macrophages (red arrowheads), lymphocytes (green arrowheads). **(b)** Percentages of the IL-5 positive area ratio in MFALCs. **(c)** Percentages of the IL-5 positive index ratio in lung tissues. Comparison between the control and diabetic groups (n = 5 mice of each group), analyzed by the Mann–Whitney *U*-test ($p \leq 0.05$). Statistically significant difference indicated by an asterisk (*). Values = mean ±SE.

Figure 11. Correlations between blood glucose level, vessel markers, and proinflammatory markers in MFALCs and the control and diabetic groups' lungs. (**a)** Spearman's correlation test for the

correlation between blood glucose level and relative area ratio of vessel markers ($CD31^+$ blood capillary and LYVE-1^+ LVs). **(b)** Spearman's correlation test for the correlation between blood glucose level and the relative ratio of proinflammatory cytokines (TNF-α and IL-5). ρ: Spearman's rank-order correlation coefficient, n = 5/group, and 10 for both groups. * Significant value, $p \leq 0.05$; ** highly significant value, $p \leq 0.01$.

Table 1: Spearman correlations between diabetic indices and parameters for both MFALCs and lung in control and diabetic mice groups.

Table 1			Parameters for diabetic indices		Parameters for MFALCs					
			Blood glucose	Insulin+ cell density	MFALC	B220	CD3	Iba1	Gr1	HEVs
Parameters for diabetic index	Blood glucose	ρ	-	-0.906**	0.796**	0.669*	0.802**	0. 769**	0.802**	0.584
		P	-	0.001	0.006	0.035	0.005	0.001	0.005	0.07
	Insulin+ cell density	ρ	-0.906**	-	-0.842**	-0.806**	-0.879**	-0.879**	-0.782**	-0.612
		P	0.001	-	0.002	0.005	0.001	0.001	0.008	0.060
Parameters for lung	Lung aniline blue positive area	ρ	0.681*	-0.685*	0.818**	0.758*	0.539	0.685*	0.709*	0.794**
		P	0.030	0.029	0.004	0.011	0.108	0.029	0.022	0.006
	Lung injury score	ρ	0.740*	-0.774**	0.774*	0.817**	0.634**	0.756**	0.591*	0.799**
		P	0.014	0.009	0.014	0.004	0.004	0.001	0.072	0.006
	B220	ρ	0.699*	-0.794**	0.673*	0.964**	0.527	0.733*	0.661*	0.818**
		P	0.024	0.006	0.033	0.001	0.117	0.016	0.038	0.004
	CD3	ρ	0.815**	-0.855**	0.952**	0.733*	0.770**	0.733*	0.758*	0.673*
		P	0.004	0.002	0.001	0.016	0.009	0.016	0.011	0.033
	Iba1	ρ	0.796**	-0.903**	0.794**	0.758**	0.855**	0.976**	0.842**	0.661*
		P	0.006	0.001	0.006	0.011	0.002	0.001	0.002	0.038
	Gr1	ρ	0.802**	-0.782**	0.855**	0.612	0. 697**	0.782**	1.000**	0.697*
		P	0.005	0.008	0.002	0.060	0.025	0.008	0.001	0.025

MFALC: % of LCs area/total MFTs area. ρ: Spearman's rank order correlation coefficient. n= 5/group (control, and diabetic groups). *: Significant, $P < 0.05$. **: highly significant, $P < 0.01$.

a) Experimental protocol

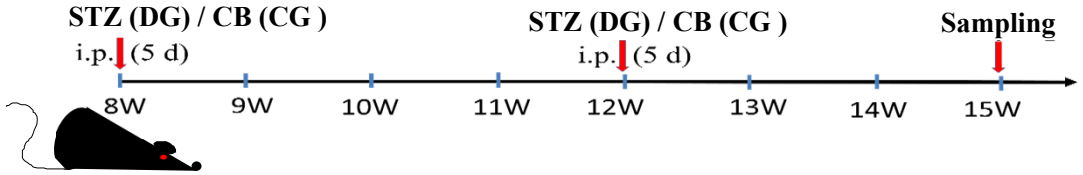

b) Blood glucose level

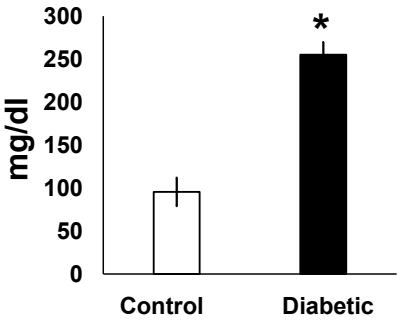

c) Immunohistochemical staining of insulin positive beta cells

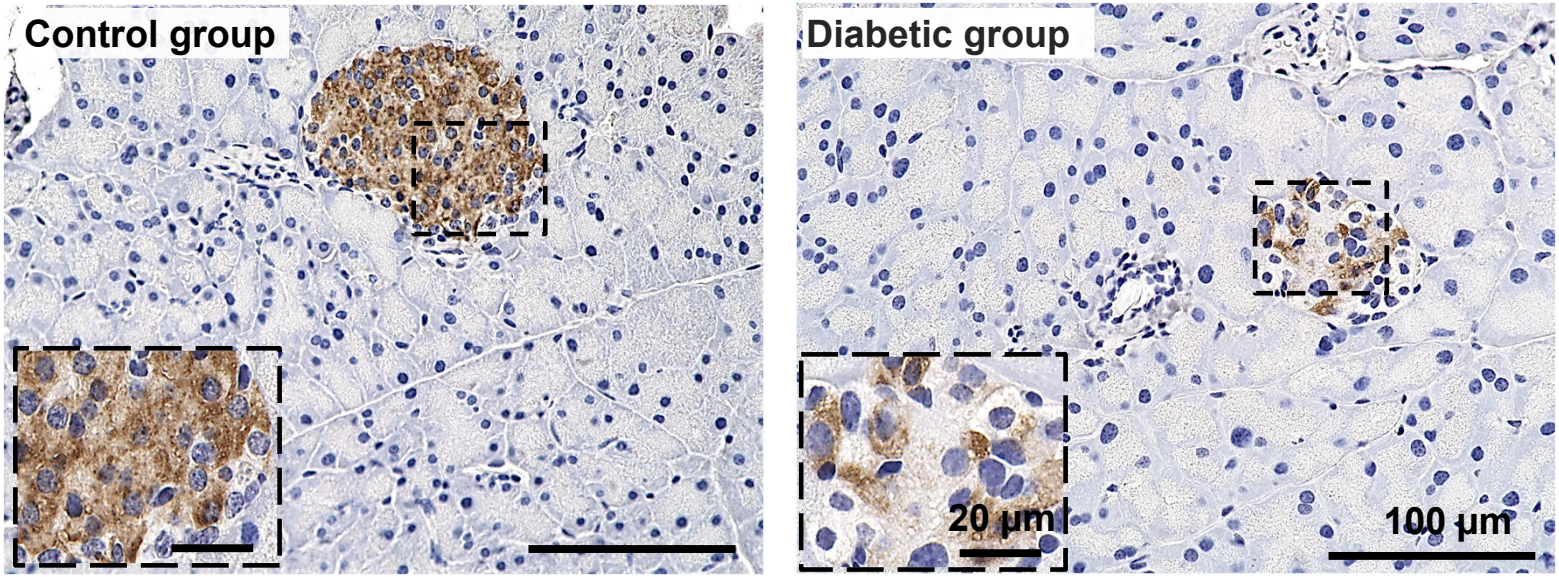

d) Ratio of islet area/ pancreatic area (μm²)

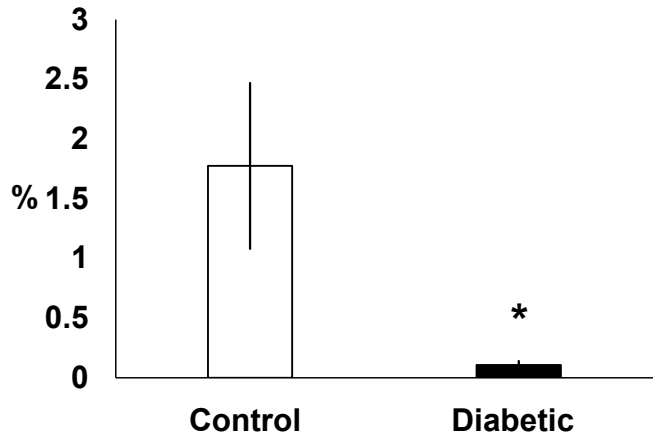

e) β- cells Index ratio (Insulin positive number/ islet area)

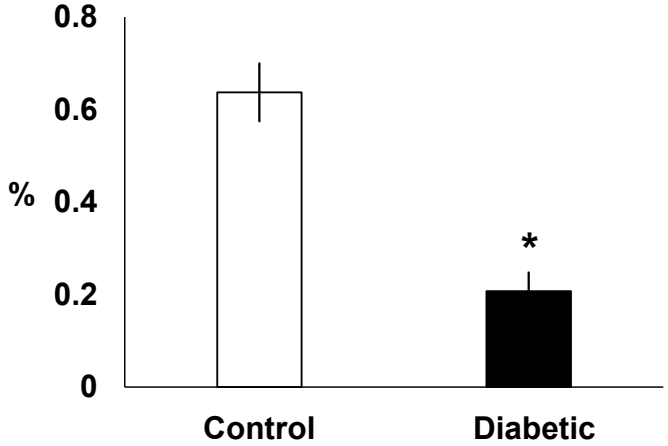

a) H&E staining of mediastinal fat tissue

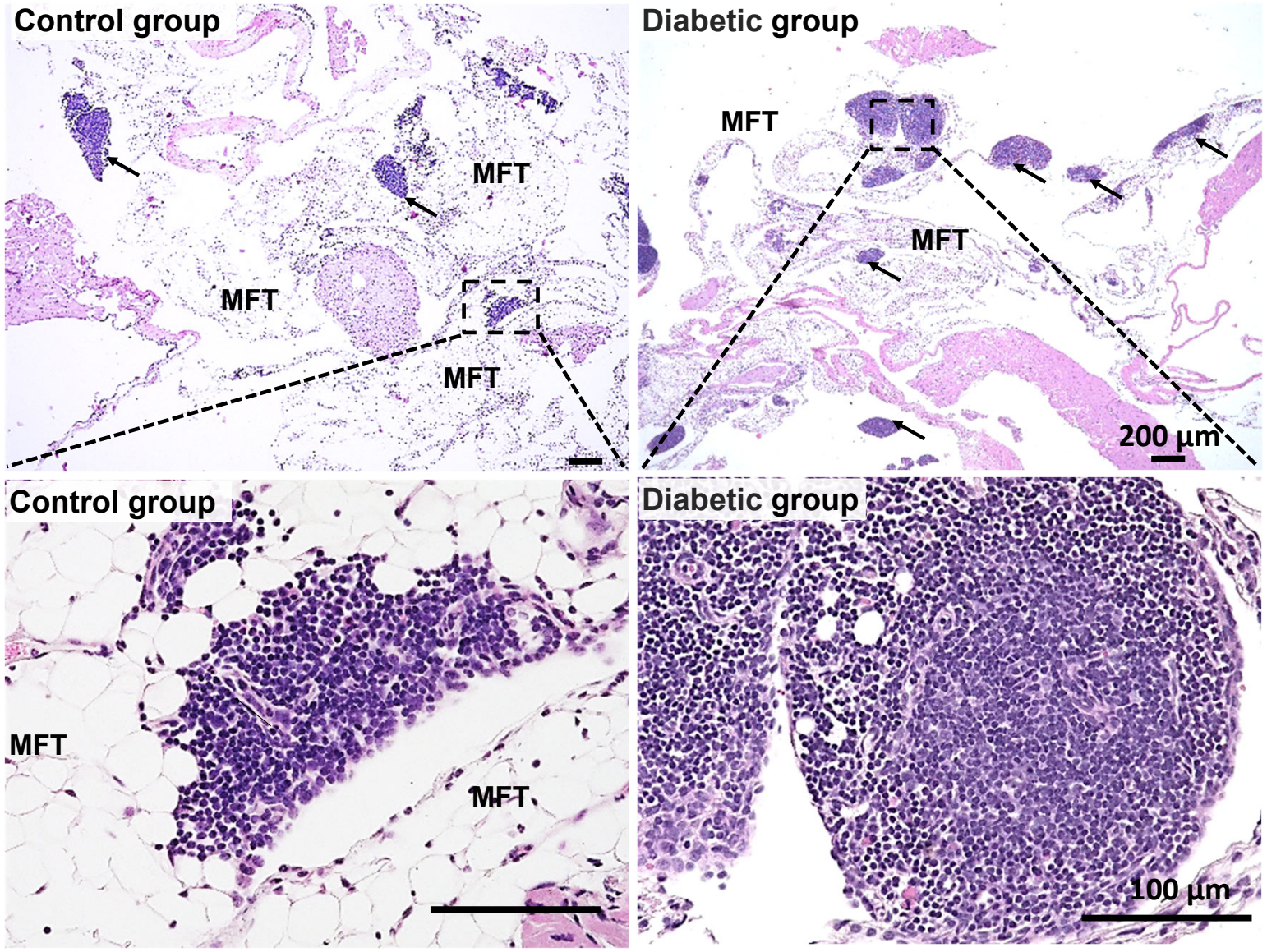

b) Ratio of lymphoid clusters area/ total MFT area (µm²)

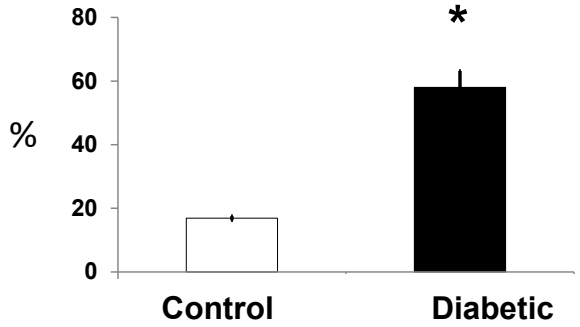

c) Spleen/ B.W. ratios

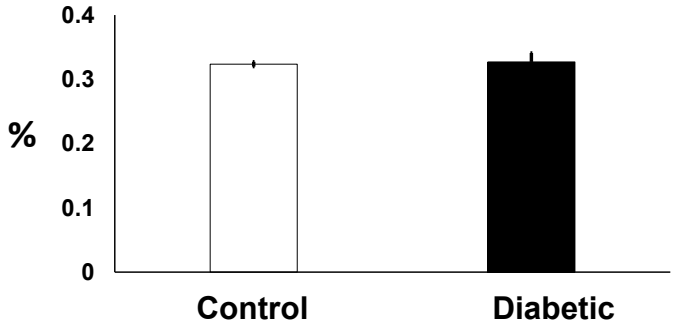

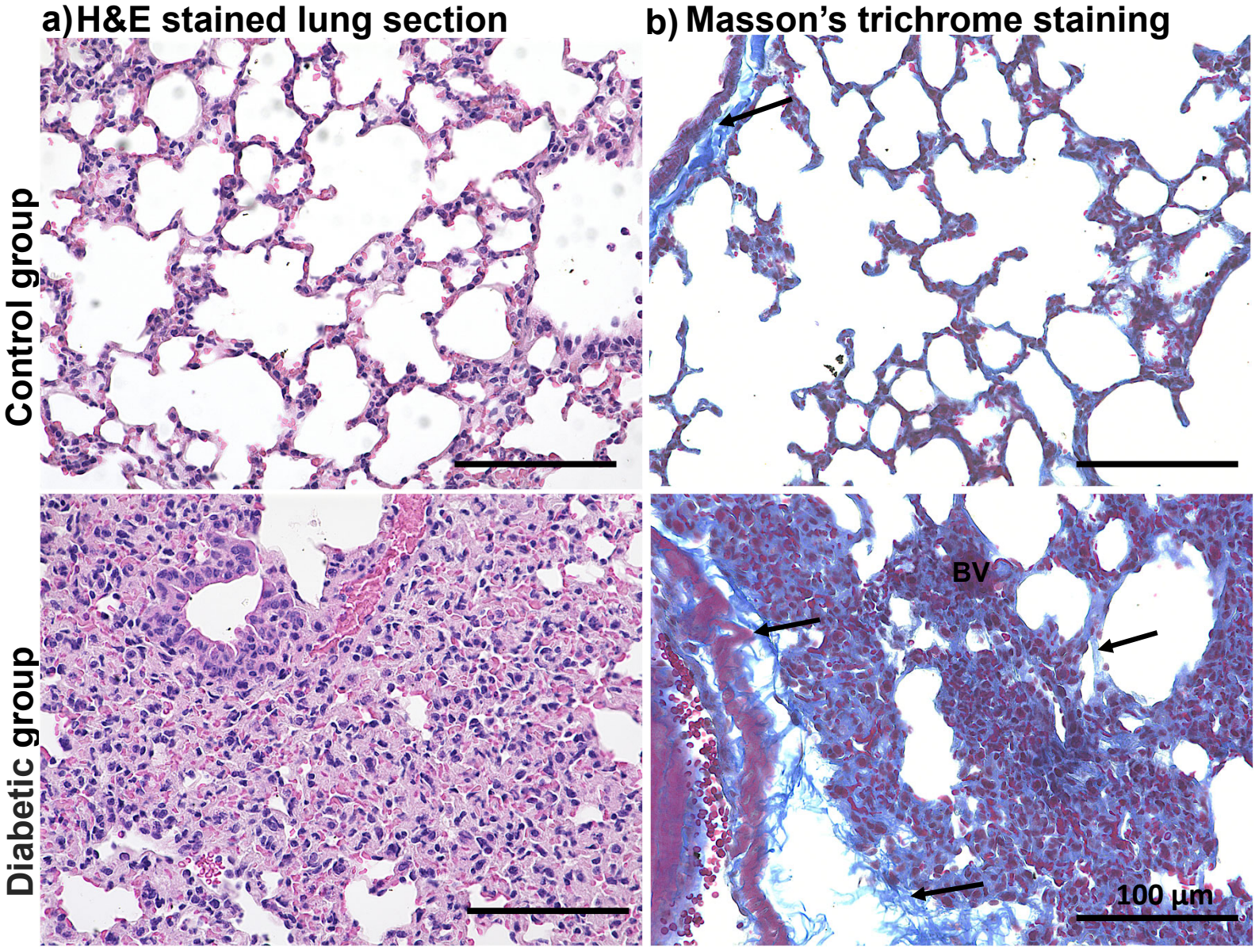
a) H&E stained lung section
b) Masson's trichrome staining
Control group
Diabetic group
BV
100 µm

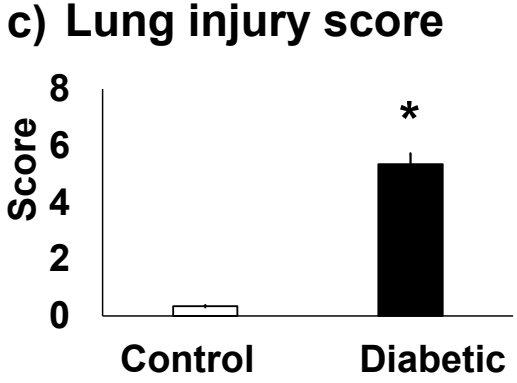
c) Lung injury score
Score
8
6
4
2
0
*
Control
Diabetic

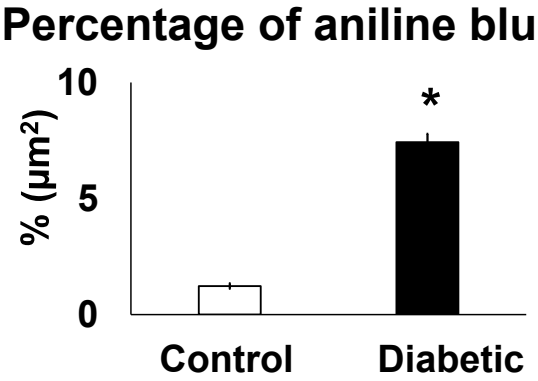
d) Percentage of aniline blue+ area
% (µm²)
10
5
0
*
Control
Diabetic

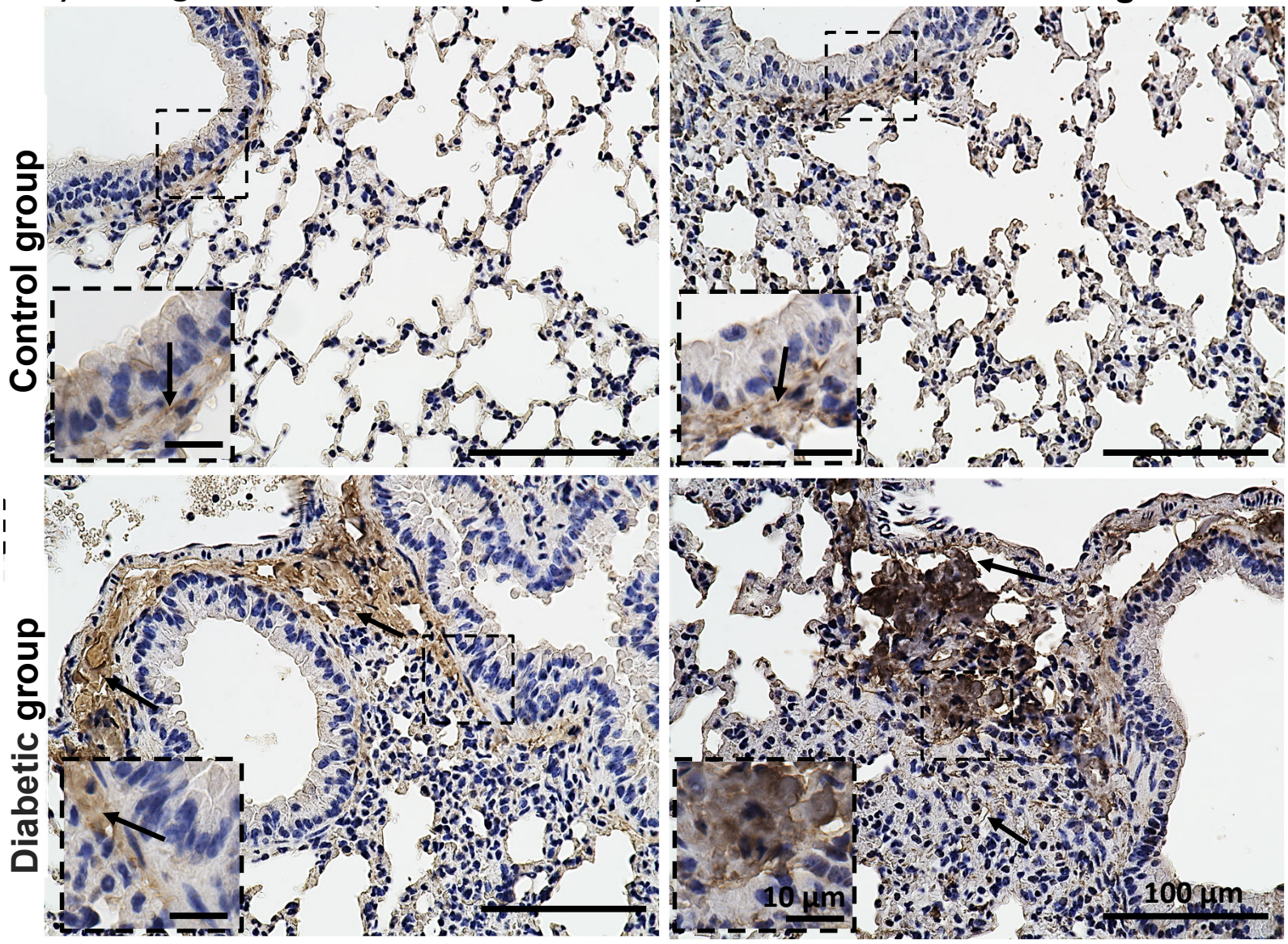
a) Collagen I immunostaining
b) Col3A1 immunostaining
Control group
Diabetic group
10 µm
100 µm

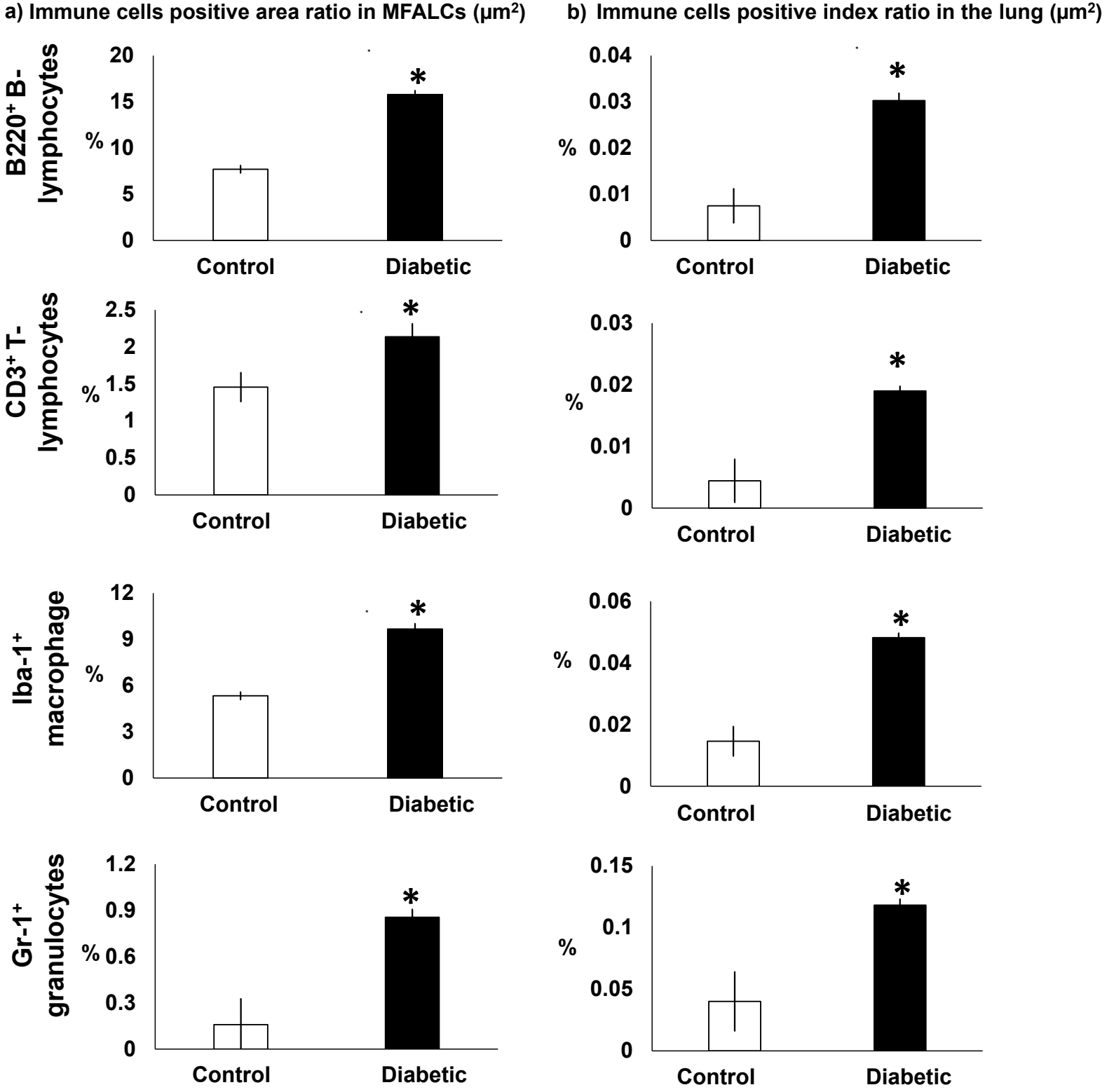
a) Immune cells positive area ratio in MFALCs (μm²)
b) Immune cells positive index ratio in the lung (μm²)
B220⁺ B-lymphocytes
CD3⁺ T-lymphocytes
Iba-1⁺ macrophage
Gr-1⁺ granulocytes
%
Control
Diabetic
*
0
5
10
15
20
0.5
1
1.5
2
2.5
3
6
9
12
0.3
0.6
0.9
1.2
0.01
0.02
0.03
0.04
0.05
0.1
0.15

a) Immunohistochemical staining of PNAd positive high endothelial venules in MFALCs and lung

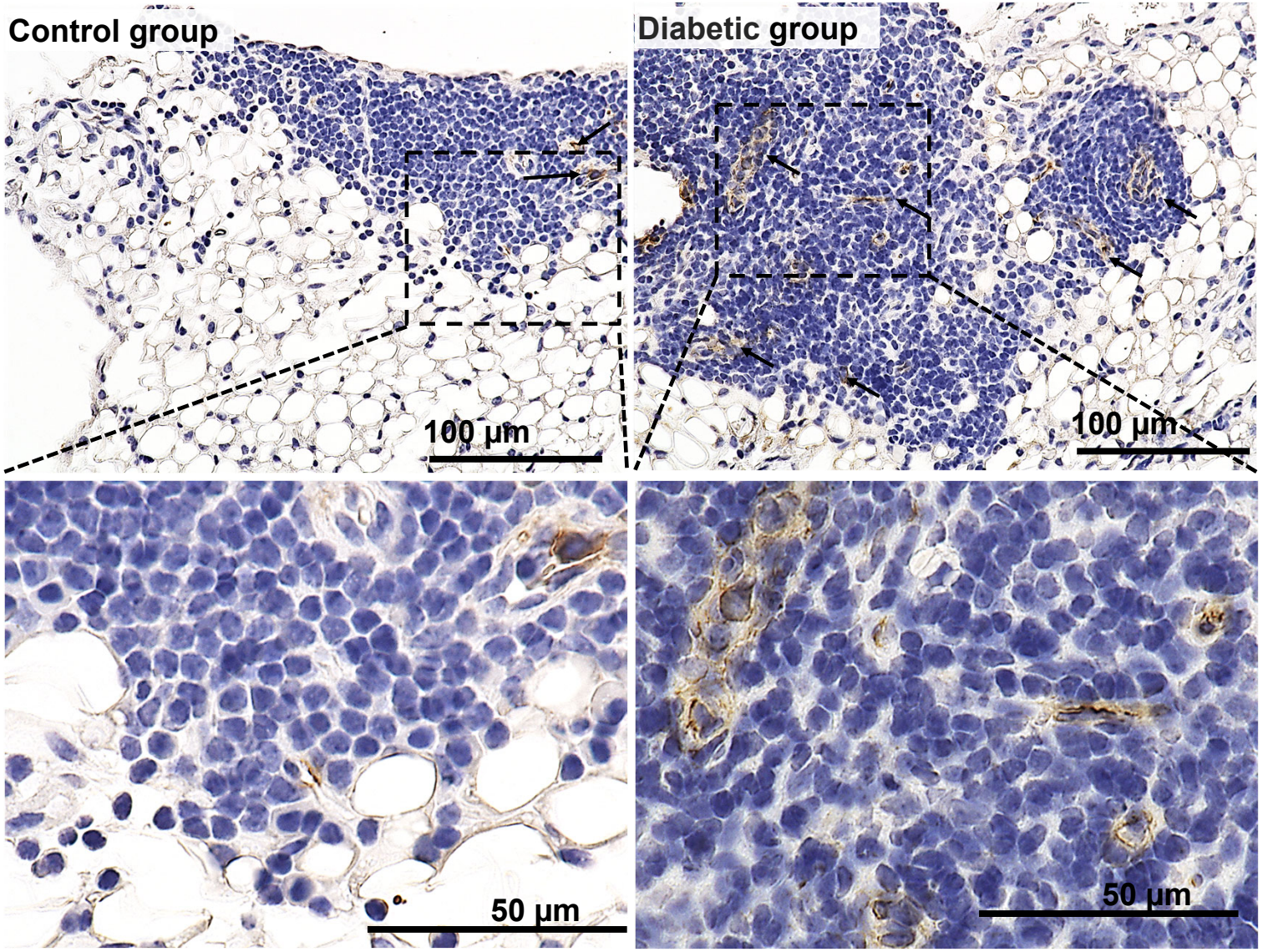

b) Ratio of HEVs area/ cluster area (μm²)

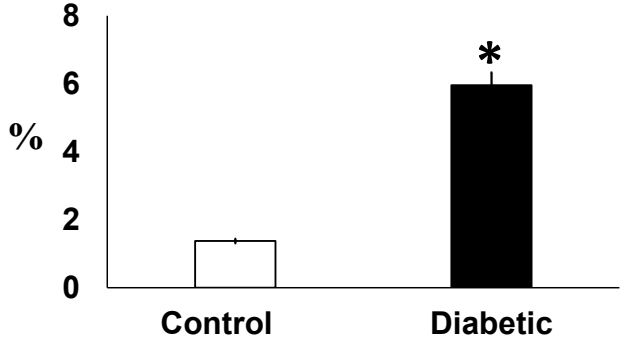

a) Immunohistochemical staining of LYVE-1 positive lymphatic vessels (LVs) in MFALCs and lung

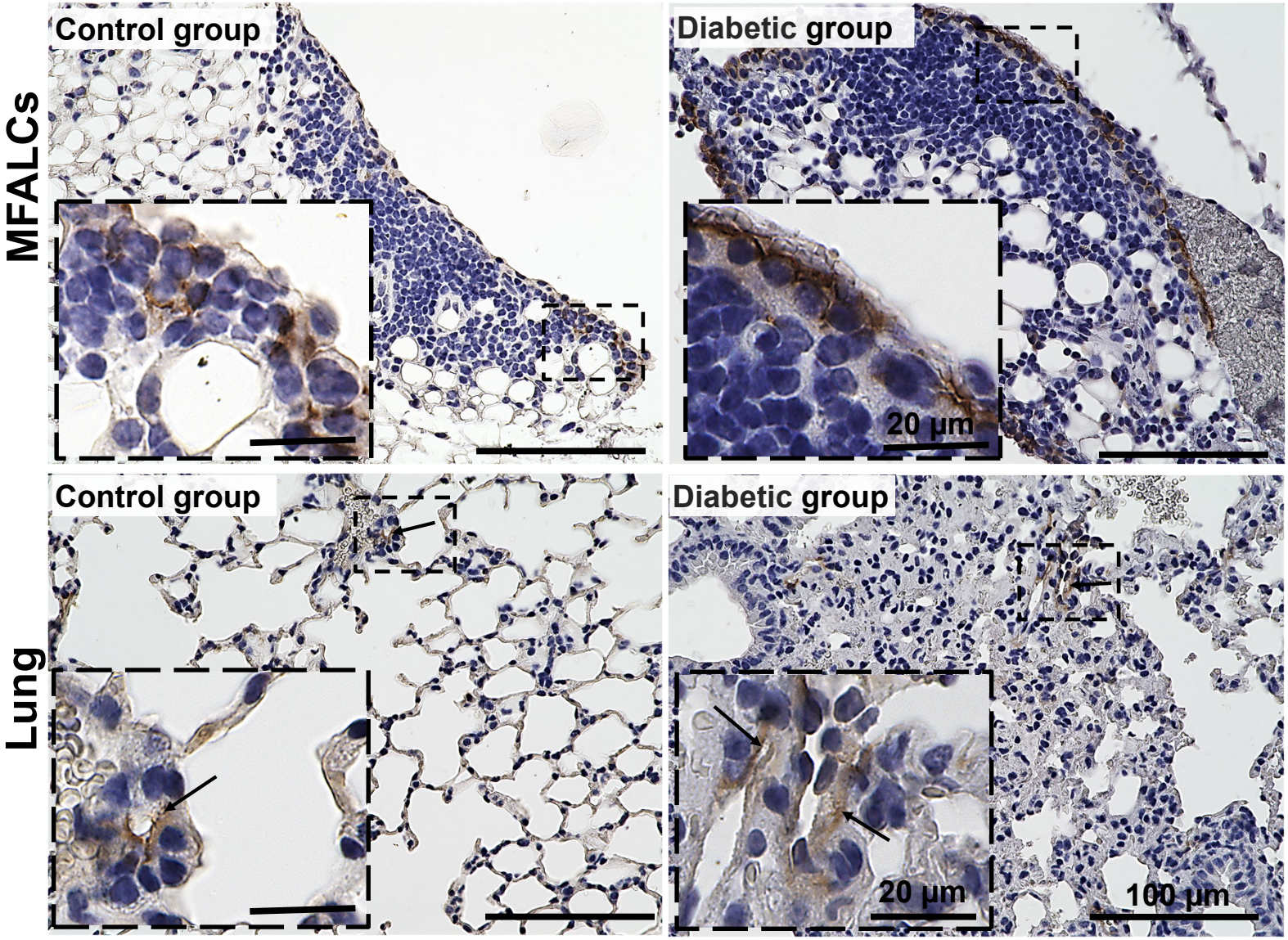

b) Ratio of LYVE-1+ LVs area in MFALCs (μm²)

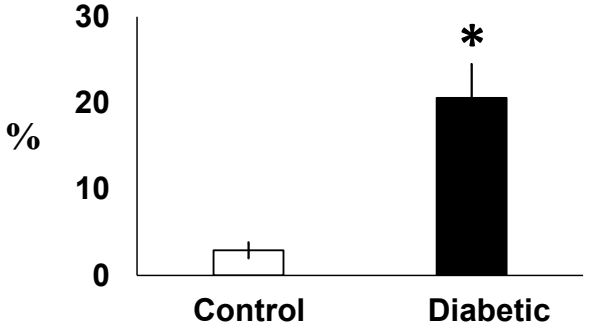

c) Ratio of LYVE-1+ LVs area in Lung (μm²)

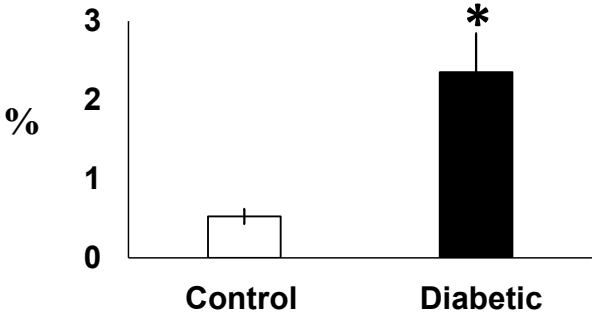

a) Immunohistochemical staining of CD31 positive endothelial cells in MFALCs and lung

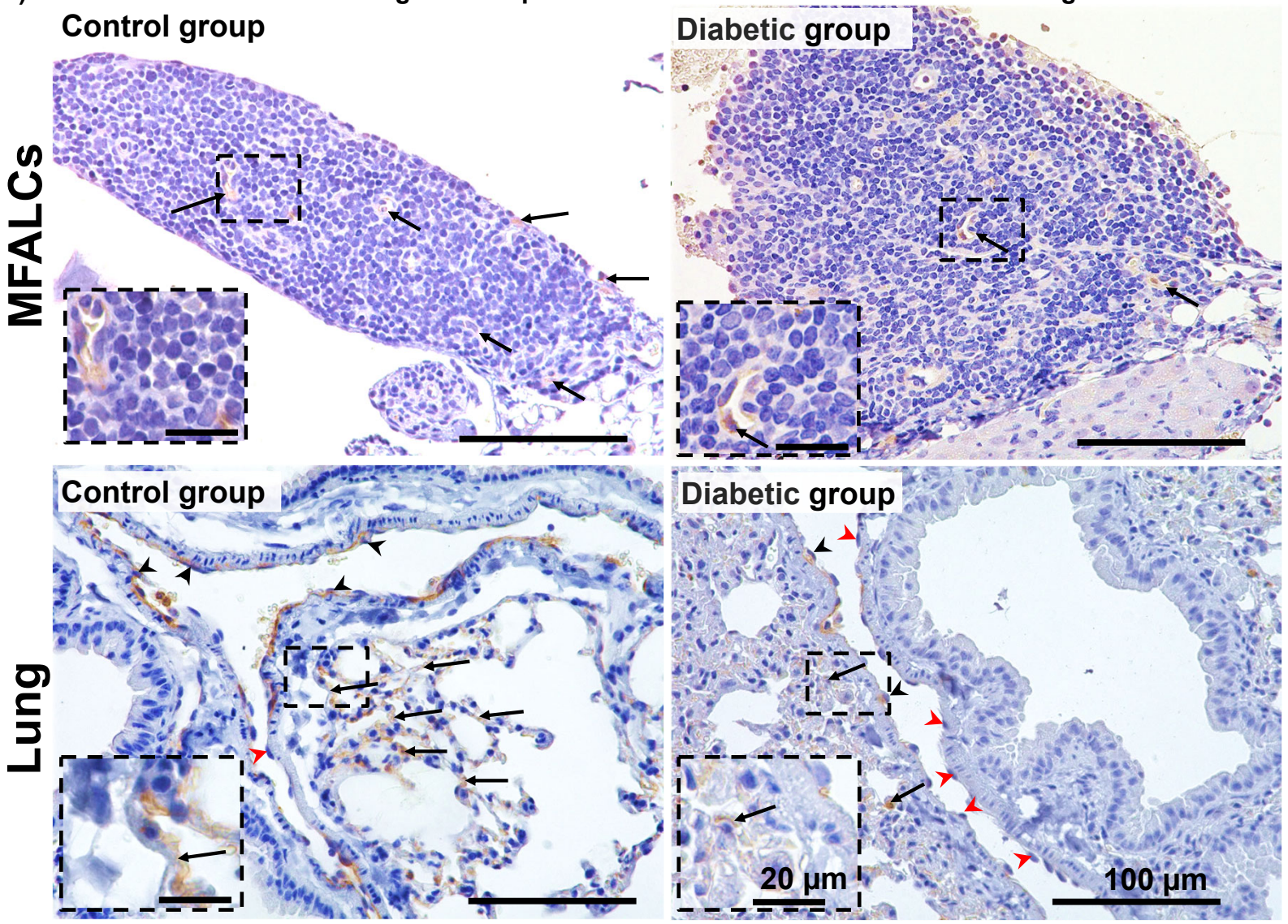

b) Ratio of CD31 area/ MFALCs area (μm²)

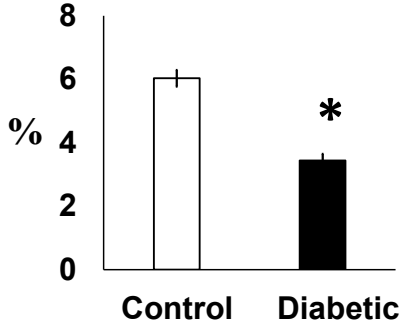

c) Ratio of CD31+ capillary area/ lung area (μm²)

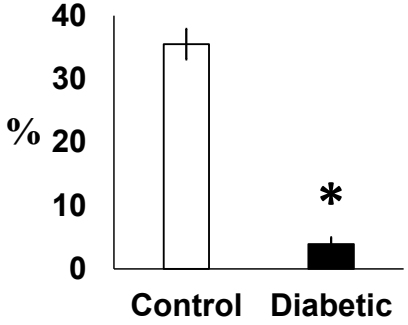

d) Index ratio of CD31+ endothelial cells /blood vessel wall within lung

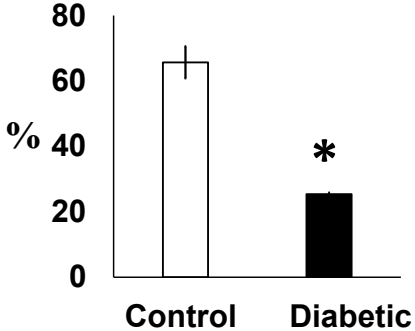

a) Immunohistochemical staining of TNF- α positive endothelial cells in MFALCs and lung

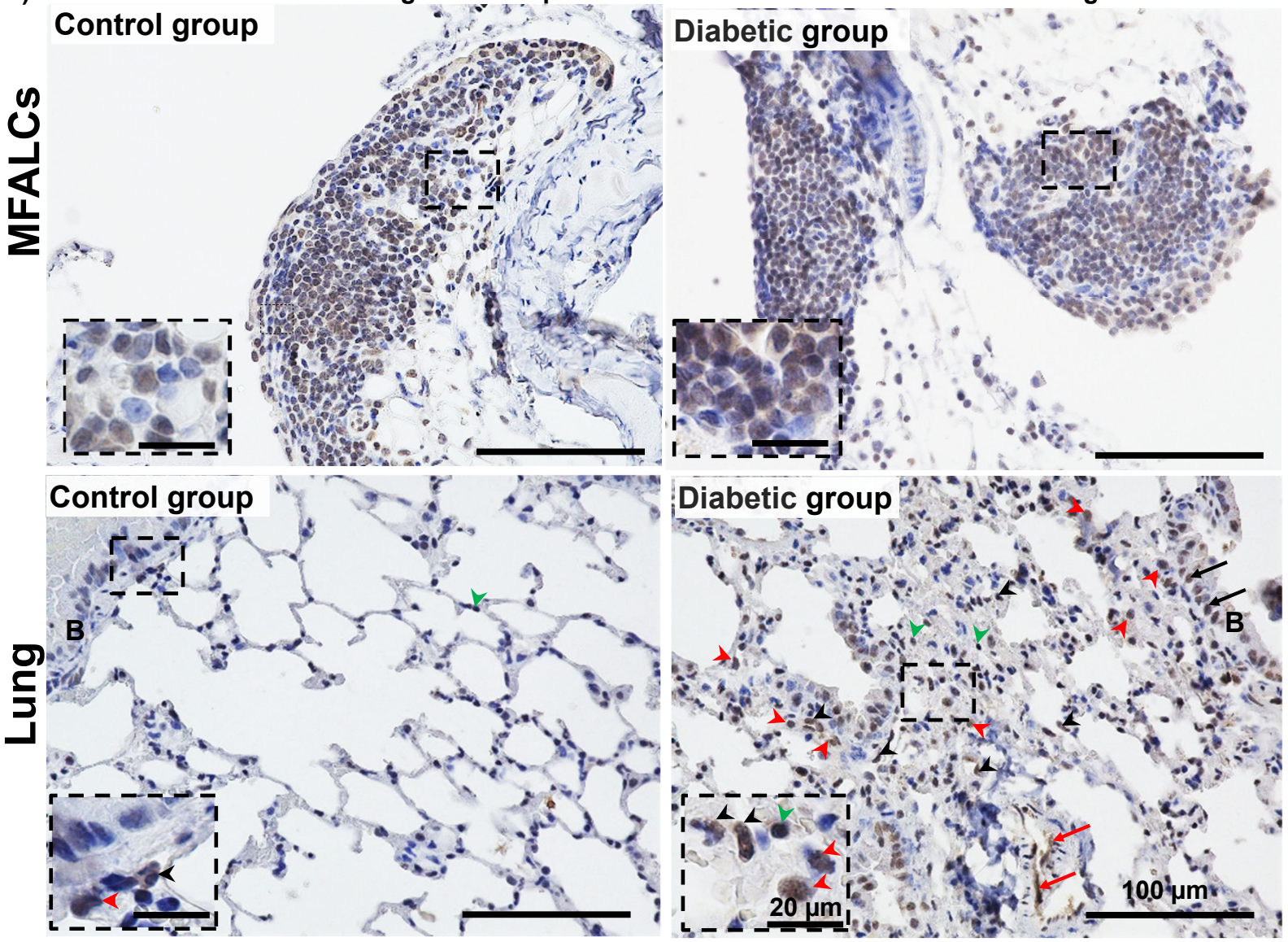

b) TNF-α positive area ratio in MFALCs (μm²)

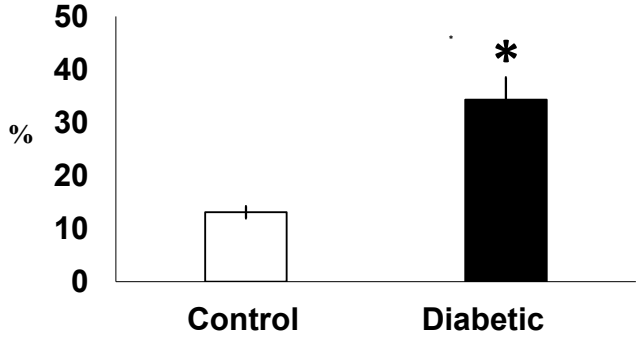

c) TNF-α positive index ratio in lung (μm²)

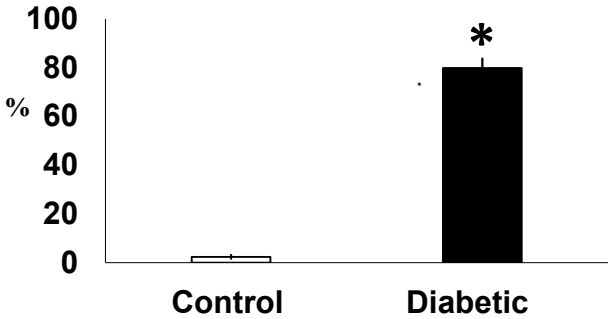

a) Immunohistochemical staining of IL5 positive endothelial cells in MFALCs and lung

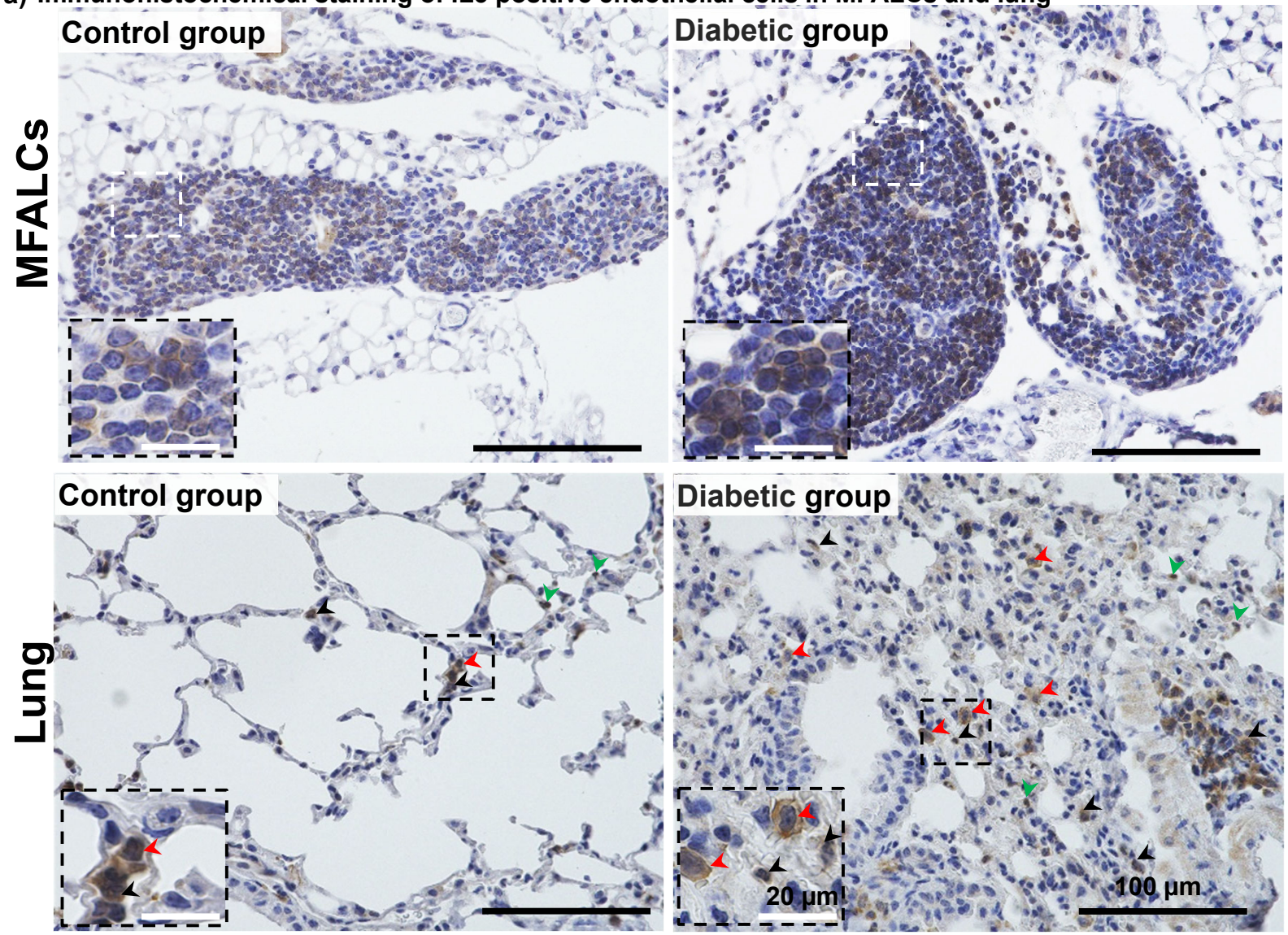

b) IL5 positive area ratio in MFALCs (μm²)

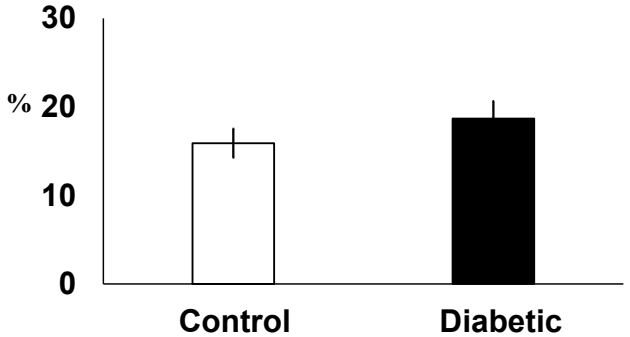

c) IL5 positive index ratio in lung (μm²)

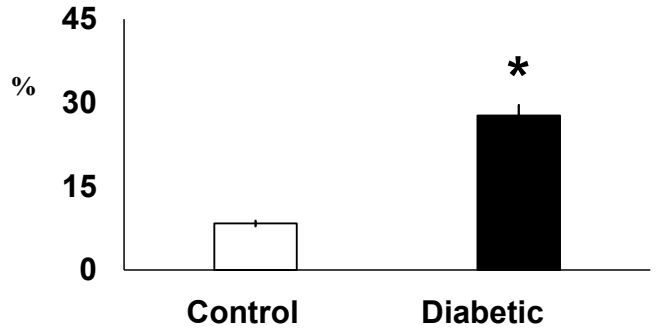

a) Correlations between blood glucose level (BGL) and expression of vessel markers.

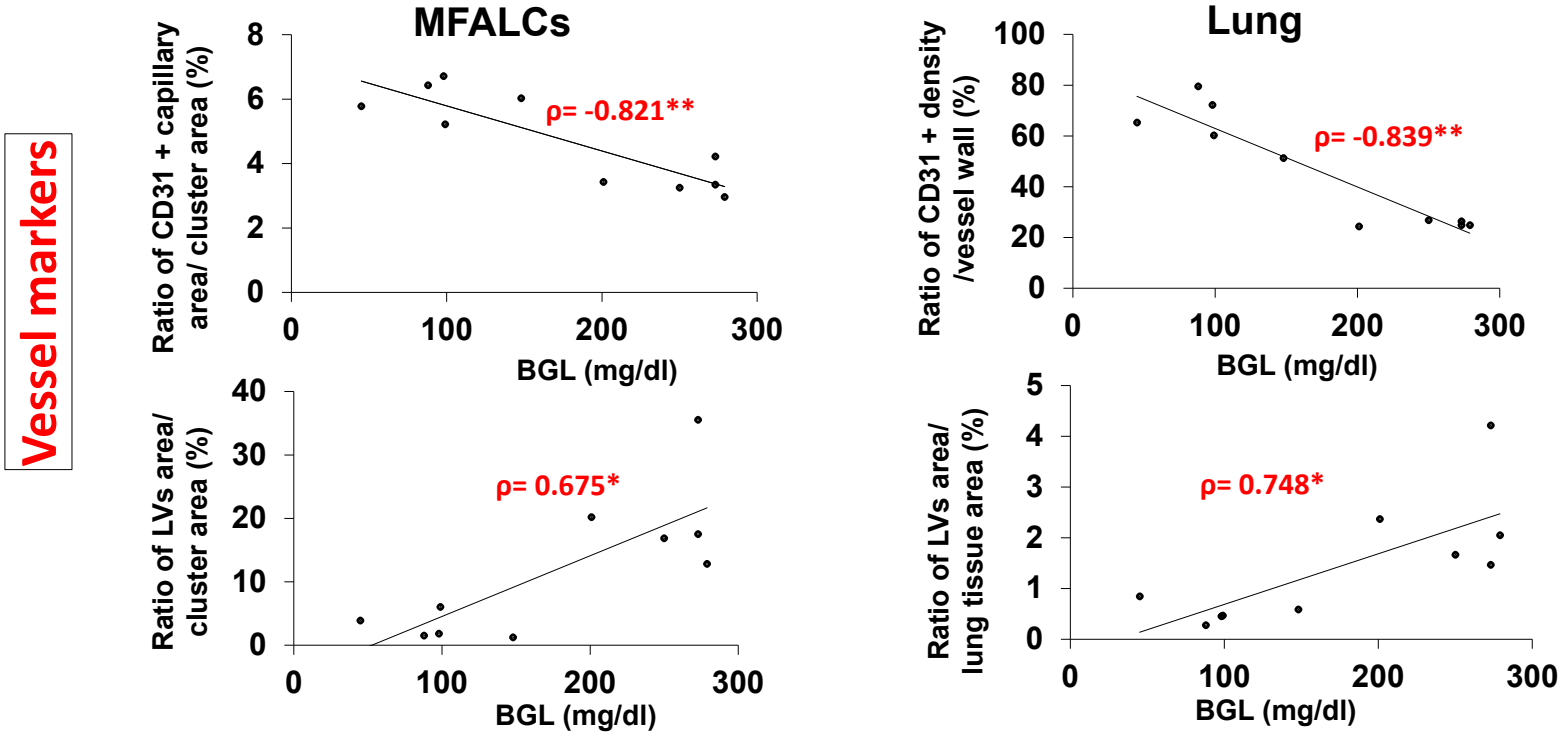

b) Correlations between blood glucose level and expression of inflammatory markers